

## 34.0 PHASE AND TEXTURE EVOLUTION PRECEDING ABNORMAL GRAIN GROWTH IN NI-BASED AEROSPACE ALLOYS

Byron McArthur (Mines)

Faculty: Amy Clarke (Mines) and Kester Clarke (Mines)

Industrial Mentors: Eric Payton (AFRL), Kevin Severs (ATI)

This project initiated in Fall 2017 and is advised by Amy Clarke and Kester Clarke at Colorado School of Mines (Mines). The research performed during this project will serve as the basis for a Ph.D. thesis for Byron McArthur.

### 34.1 Project Overview and Industrial Relevance

Nickel-based superalloys are utilized extensively in the aerospace industry for their excellent high temperature strength, fatigue life, oxidation resistance and corrosion resistance. Turbine engine discs are flight critical components, and failure of these components risk loss of the entire plane. With the continuous push for more efficient commercial aviation, higher operating temperatures and pressures are desired. Complex Ni-based superalloys are being processed through novel methods to meet these stringent requirements.

The alloy utilized in the present study is RR1000, a  $\gamma$ - $\gamma'$  disk alloy with approximately 45% volume fraction of  $\gamma'$  at room temperature. Processing steps include alloyed powderization, hot isostatic pressing and extrusion at a 4.5:1 reduction ratio [34.1]. These steps produce a fully dense, recrystallized billet with  $\gamma$  grain size of 1-5  $\mu\text{m}$  diameter and a distribution of primary  $\gamma'$  ( $\gamma_1'$ , 1-3  $\mu\text{m}$ ) and secondary  $\gamma'$  ( $\gamma_2'$ , 20-50 nm). Two material conditions provided are shown in **Figure 34.1**, note the significant difference in fraction of  $\gamma_1'$ . Subsequent isothermal deformation processing of slices of material is performed near the  $\gamma'$  solvus temperature;  $\gamma_2'$  is dissolved while  $\gamma_1'$  pins the  $\gamma$  grain boundaries and superplastic deformation keeps flow stresses low. Super-solvus heat treatment (SSHT) allows for  $\gamma$  growth to approximately 50  $\mu\text{m}$  for increased creep resistance during service [34.1]. Abnormal grain growth (AGG) has been shown to occur during the SSHT based upon processing parameters in the isothermal deformation ( $\epsilon$ ,  $\dot{\epsilon}$ , T) and SSHT heating rate. The AGG results in  $\gamma$  grains up to 3 mm that compromise mechanical performance and are difficult to detect via non-destructive testing. The objective of this project is to better understand the microstructural mechanisms that cause AGG in these materials through use of advanced, in-situ experimental techniques.

### 34.2 Previous Work

#### 34.2.1 Literature Review

Prior research into AGG has been most successful in exploring the processing parameters required to produce AGG in an effort to prevent the phenomena from occurring in industrial components. Huron et al. [34.2] performed double cone isothermal compression testing on a similar alloy (René 88DT) and found a range of strain rates and deformation temperatures that produce AGG; increasing deformation temperature required higher strain rates to produce AGG. Parr et al. [34.3] did similar testing on RR1000 and found AGG conditions to occur at near- $\gamma'$ -solvus deformation temperatures, low strain rates, and low strains; similar to those explored in the present study. In-depth work performed by Payton [34.4] explored characterization techniques in an effort to understand the microstructural mechanism behind AGG; results indicated stored energy within the  $\gamma$  grains was a likely contribution to AGG, however combined contributions from  $\gamma'$  coherency changes and redistribution are important as well.

Work further exploring the AGG mechanisms has been performed by Charpagne et al. [34.5], and proposes that stored energy is the driving force for AGG, with static recrystallization of  $\gamma$  grains initiating the process. The recrystallization of the  $\gamma$  grains has been proposed by Charpagne to occur coherently off of  $\gamma_1'$ , preceded by growth to consume neighboring  $\gamma$  grains containing stored energy; this mechanism has been termed 'heteroepitaxial recrystallization' (HERX). The coherency allows for a reduced energy barrier for recrystallization of the  $\gamma$ , theoretically occurring at lower temperatures. Interestingly, the  $\gamma$  grain boundaries appear to pass through large  $\gamma_1'$  with relatively low Zener pinning influence. Charpagne's work demonstrated continued growth of  $\gamma$  grains within critical regions until impingement upon each other limited grain growth. This suggests the final grain size is determined by the number of nucleation sites that then grow to consume regions of unrecrystallized grains. The nucleation limited growth may be explained by inhomogenous distributions of stored energy that is a precursor to static recrystallization. Tu et al.'s work [34.6] supports this through strain mapping characterization techniques demonstrating significant grain-to-grain

variations in plastic strain accumulation as well as changes in deformation mechanisms near the critical strain rates required for AGG. Based upon prior research, it appears that stored energy, accumulated inhomogeneously during isothermal forging, creates the precursor requirements for AGG.

### 34.2.2 Thermomechanical Processing to Produce Abnormal Grain Growth

Prior experiments in this study focused on establishing the thermomechanical processing parameters for consistently producing AGG in the experimental RR1000 materials. The main portion of this research so far has focused on the material with the starting condition shown in **Figure 34.1a**, containing a lower fraction of  $\gamma_1'$ , smaller  $\gamma_2'$  and larger  $\gamma$  grains, as this material has shown instances of AGG during testing. Thermomechanical processing of the material with the starting condition shown in **Figure 34.1b** has not yet demonstrated instances of AGG. This is likely due to increased amounts of  $\gamma_1'$  influencing the deformation and recrystallization.

Isothermal compression of RR1000 specimens was performed in a Gleeble® thermomechanical simulator. This allowed for control of deformation temperature, strain, and strain rate as well as providing load-displacement data. Post-deformation SSHT of the material utilized a TA Instruments quenching dilatometer to maintain precise temperature and heating rate control, as well as measure qualitative  $\gamma'$  dissolution and  $\gamma$  grain growth behavior through changes in length. The deformation temperature, strain rate, and strain utilized in the Gleeble® to produce AGG were 1110°C, 0.0008  $\epsilon/s$  and 0.16  $\epsilon$ , respectively. This is just below the 1135-1145°C  $\gamma'$  solvus temperature. Utilizing the dilatometer, a low heating rate (0.12°C/s) up to the SSHT temperature (1170°C) promoted AGG occurrence.

Interrupted heat treating was utilized in an attempt to approach in-situ observation capabilities of the sequence of AGG. A region of the material from the axisymmetrically similar region (with regard to forging temperature, strain, and strain rate) in the Gleeble samples that created AGG conditions was used for interrupted heat treating and scanning electron microscopy – electron backscattered diffraction (SEM-EBSD) characterization. Post heat-treatment microstructures between the specimen utilized for interrupted heat treating and non-interrupted heat treating were compared and confirmed the interruption process of cooling and reheating did not influence final results. SEM-EBSD mapping results following the same spatial region are shown in **Figure 34.2** for conditions of (a) as forged at 1120°C to 0.15 strain and 1E-3 strain, followed by heat treating to temperatures of (b) 1130°C, (c) 1150°C, and (d) 1170°C at a heating rate of 0.13°C/s; note the grain coloring changes in **Figure 34.2c** due to specimen rotation issues. Interestingly, significant AGG occurs below the  $\gamma'$  solvus temperature, indicating the remaining  $\gamma_1'$  provides insufficient Zener pinning force to prevent AGG of  $\gamma$ . As expected, the  $\gamma$  growth continues until the abnormally large grains impinge upon each other, with remaining  $\gamma$  grains being consumed at higher temperatures. Interestingly, the grain boundary of the abnormally large  $\gamma$  appears capable of passing around existing  $\gamma$  grains and fully encapsulating them, as observed in **Figure 34.2**. Multiple instances of this have been observed in various specimens undergoing AGG, and it is believed to not be just an instance of sectioning effects.

If AGG does indeed occur as a result of the theorized HERX mechanism, as these initial findings suggest, the  $\gamma_1'$  phase fraction, size, and distribution are of importance. While the  $\gamma_2'$  are likely dissolved at isothermal forging and heat treating temperatures, the  $\gamma_1'$  exists and serves as AGG nuclei location sites.

## 34.3 Recent Progress

### 34.3.1 Microstructural Modeling

Microstructural evolution modeling of the  $\gamma'$  dissolution in a  $\gamma$  matrix was performed to analyze the effects of possible spatial clustering of a precipitate on the grain size distribution of the  $\gamma$ . In regions of higher  $\gamma'$  spatial clustering,  $\gamma'$  dissolution changes the matrix composition to reduce local dissolution rates, resulting in regions of  $\gamma'$  remaining to pin clusters of  $\gamma$  grains. This theory of soft impingement producing a bimodal grain size was explored using a kinetic Monet Carlo simulator. Sandia National Laboratories created this modeling software, Stochastic Parallel PARTicle Kinetic Simulator (SPPARKS), with a hybrid Potts-Phase Field application for simulating two phase microstructural evolution [34.7]. This modeling allows for an input initial microstructure, with two defined phases and composition to evolve towards equilibrium. The Potts model is a Monte Carlo based progression of statistically allowing site flipping based upon probability and state equations to describe the energy of the system. Energetically favorable changes (that reduce the energy of the system) are chosen from a list of possible selections and accepted, while a Boltzman temperature term allows for energetically unfavorable changes to occur; based upon an Arrhenius equation.

The phase field model is a continuum model rather than discrete, and uses state equations that take into account the bulk free energy, interfacial energy, and composition gradients. Iterative steps serve as a metric of time while performing Potts model and phase field model calculations for all sites. While the model serves to allow in-situ-like observation of the evolution of a microstructure, the limitations of the model must be acknowledged. The state equations are non-dimensionalized and the system is unitless, thus cannot be applied directly to real world systems. The Boltzman temperature only influences the entropic component of the system, while the bulk free energy of the system is defined by phenomenological constants.

A starting microstructure of  $\gamma'$  embedded in  $\gamma$  was created using Dream.3D. Spatial clustering of the  $\gamma'$  was performed by using a radial distribution function, then overlaying onto an existing, randomly distributed  $\gamma'$  in  $\gamma$  matrix. A Gaussian distribution was applied to the  $\gamma$  and  $\gamma'$  grains, with compositions predefined in each phase. The phenomenological input parameters to modify the thermodynamics and kinetics of the system were iteratively tested to create a system with  $\gamma'$  dissolution and  $\gamma$  growth rates approximating experimental results. The spatial clustering of the  $\gamma'$  creates local concentrations of solute during dissolution, seen in **Figure 34.3a**, that locally retard the remaining  $\gamma'$  from dissolving. The soft impingement of the pinning  $\gamma'$  disrupts  $\gamma$  grain growth to create a bimodal grain size, seen in **Figure 34.3b**.

#### 34.4 Plans for Next Reporting Period

Ongoing work is focused on refining the temperature resolution of the interrupted heat treated specimen testing to better track the progression of AGG and interaction with neighboring grains. Temperature ranges will focus on the sub-solvus regimes to include  $\gamma_1'$ . In addition to SEM-EBSD, SEM-EDS (electron dispersive spectroscopy) may assist in detecting  $\gamma_1'$  coherent with the  $\gamma'$  matrix (resolvable via local depletions of chromium) exist for HERX nuclei. Determining the conditions for HERX, whether dynamic recrystallization or static recrystallization with a possible incubation time, will also be evaluated during these interrupted heat treating specimens. Ideally, these experiments will capture and track the AGG nuclei growth. These interrupted 2-D experiments are precursors to develop (and evaluate existing) mechanistic theories and experimental procedures for in-situ 3-D and diffraction experiments.

Fraction, size, and distribution of remaining  $\gamma_1'$  in undeformed specimens will be explored. Additionally, the specimens deformed at various strain rates will be evaluated to determine effect of high temperature strain on  $\gamma_1'$  stability.

#### 34.5 References

- [34.1] M. C. Hardy, B. Zirbel, G. Shen, R. Shankar. Developing damage tolerance and creep resistance in a high strength nickel alloy for disc applications, *Superalloys 2004* 83 (2004).
- [34.2] E. Raymond, E. Huron, S. Srivasta. Control of grain size via forging strain rate limits for R'88DT, *Superalloys 49* (2000).
- [34.3] I. M. D. Parr, T. J. Jackson, M. C. Hardy, D. J. Child, C. Argyrakis, K. Severs, V. Saraf, J. M. Stumpf. Inhomogeneous grain coarsening behavior in supersolvus heat treated nickel-based superalloys RR1000, *Superalloys 447* (2016).
- [34.4] E. J. Payton, Characterization and modeling of grain coarsening in powder metallurgical nickel-based superalloys, The Ohio State University, 2009.
- [34.5] M. A. Charpagne, J. M. Franchet, N. Bozzolo. Overgrown grains appearing during sub-solvus heat treatment in a polycrystalline  $\gamma$ - $\gamma'$  Nickel-based superalloy, *Mater. Des.* 144, 353 (2018).
- [34.6] W. Tu, T. M. Pollock. Grain scale straining processes during high temperature compression of a PM disk alloy, *Superalloys 395* (2008).
- [34.7] E.R. Homer, V. Tikare, E.A. Holm, Hybrid Potts-phase field model for coupled microstructural – compositional evolution, 69 (2013) 414–423. doi:10.1016/j.commat.2012.11.056.

## 34.6 Figures and Tables

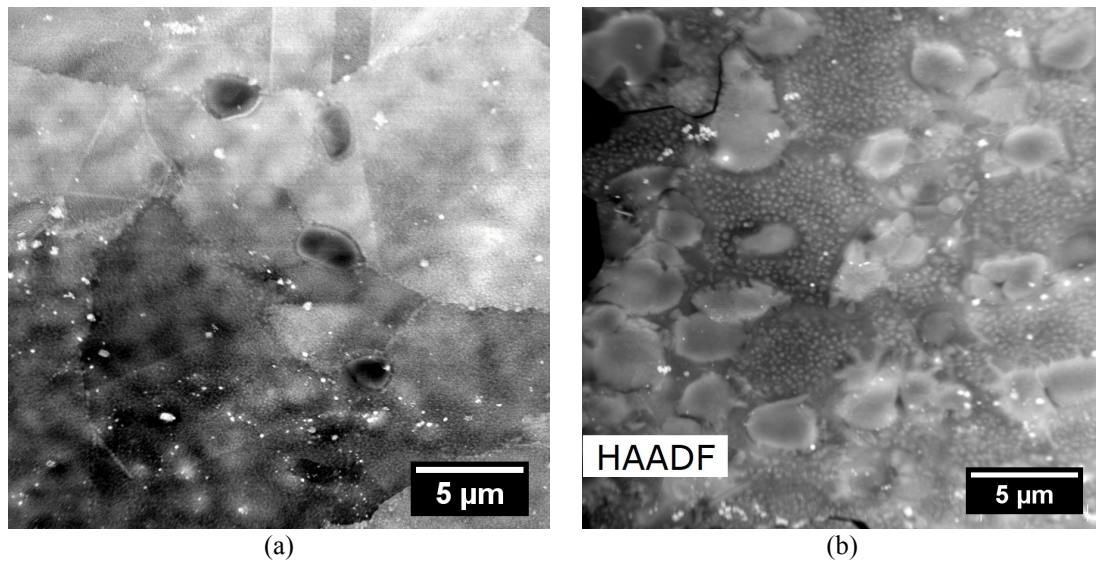


Figure 34.1: TEM micrographs of starting material conditions for 'Slice' 1 (a) and 2 (b). Slice 1 has  $\gamma_1'$  shown in darker regions, with  $\gamma_2'$  dispersed throughout the  $\gamma$  grains. Slice 2 shows higher volume fraction of  $\gamma_1'$  and larger  $\gamma_2'$ . Note the lighter regions are likely carbides remaining in the material as well as redeposited during electropolishing.

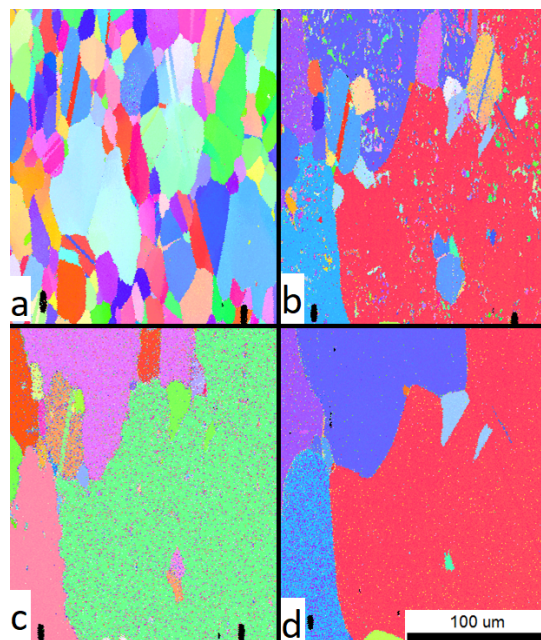


Figure 34.2: SEM-EBSD map of a constant region progressing through abnormal grain growth. Micrographs illustrate (a) as-forged microstructure (b) heated to 1130°C (c) 1150°C (d) 1170°C. Note that the  $\gamma'$  solvus temperature is nominally 1135°C. Additionally, SEM-EBSD image quality was reduced due to insufficient removal of surface oxidation with mechanical polishing techniques, as particularly seen in artifacts of micrograph (b).

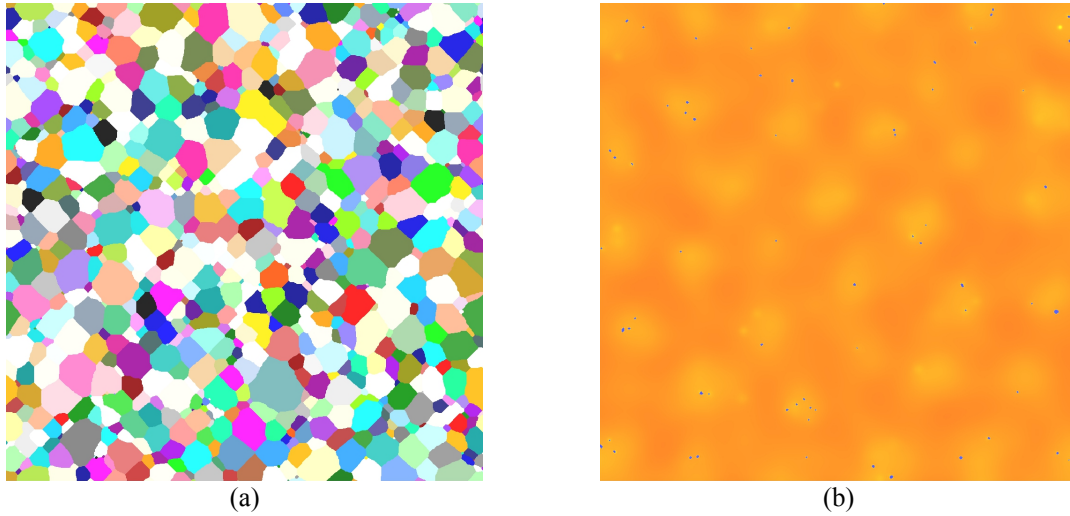


Figure 34.3: Modeling results showing a partially evolved microstructure. Individual grains are denoted by different colors in (a), while relative composition magnitudes are denoted by color in (b). Note the regions of higher composition (yellow) have remaining precipitates (blue), while precipitates in the lower concentration are completely dissolved. Additionally, these regions maintain a smaller matrix grain size, seen in (a).